frontiers | Frontiers in Earth Science

ORIGINAL RESEARCH
published: 07 July 2022
doi: 10.3389/feart.2022.916069

Kinematic Analysis of the 2020 Elliot Creek Landslide, British Columbia, Using Remote Sensing Data

Davide Donati[1]*, *Doug Stead*[2], *Marten Geertsema*[3], *Jacob M. Bendle*[4], *Brian Menounos*[4,5] *and Lisa Borgatti*[1]

[1]Dipartimento di Ingegneria Civile, Chimica, Ambientale e Dei Materiali, Alma Mater Studiorum–Università di Bologna, Bologna, Italy, [2]Department of Earth Sciences, Simon Fraser University, Burnaby, BC, Canada, [3]British Columbia Ministry of Forests, Lands, Natural Resource Operations and Rural Development, Victoria, BC, Canada, [4]Department of Geography, Earth, and Environmental Sciences, University of Northern BC, Prince George, BC, Canada, [5]Hakai Institute, Campbell River, BC, Canada

The 2020 Elliot Creek landslide-tsunami-flood cascade originated from an 18.3 Mm^3 rock slope failure in quartz diorite bedrock in a valley undergoing rapid glacial retreat. We used airborne LiDAR and optical imagery to characterize the slope and its surroundings. Using the LiDAR, we determined that two rockslides (2020 and an older undated one) occurred on this slope and shared a common basal rupture surface. We mapped two main sets of lineaments that represent structures that controlled the orientation of the lateral and rear release surfaces. Analysis of the topographic profile indicates a wedge-shaped failure block and a stepped rupture surface. Further topographic profile analysis indicates the possibility of a structurally controlled geomorphic step in the valley that corresponds with a change in the orientation of the valley. The rapid retreat of the West Grenville Glacier and the positions of the rupture surfaces suggest glacial retreat played a role in the landslides.

Keywords: elliot creek landslide, slope kinematics, remote sensing, glacier retreat, natural hazard

OPEN ACCESS

Edited by:
Hans-Balder Havenith,
University of Liège, Belgium

Reviewed by:
Alan Rempel,
University of Oregon, United States
Adam Emmer,
University of Graz, Austria

***Correspondence:**
Davide Donati
davide.donati17@unibo.it

Specialty section:
This article was submitted to Geohazards and Georisks, a section of the journal Frontiers in Earth Science

Received: *08 April 2022*
Accepted: *14 June 2022*
Published: *07 July 2022*

Citation:
Donati D, Stead D, Geertsema M, Bendle JM, Menounos B and Borgatti L (2022) Kinematic Analysis of the 2020 Elliot Creek Landslide, British Columbia, Using Remote Sensing Data. Front. Earth Sci. 10:916069. doi: 10.3389/feart.2022.916069

1 INTRODUCTION

The stability of rock slopes in alpine, mountainous regions is controlled by many geological and environmental factors. The geometrical characteristics of discontinuities at various scales (e.g., orientation, persistence, spacing of faults, joints, foliation planes), as well as ductile deformation features (e.g., the orientation of the limbs and axis of geological folds) can define the size, shape, and failure mechanism of potentially unstable blocks (Agliardi et al., 2001; Badger 2002; Brideau and Stead 2012; Stead and Wolter 2015). The mechanical properties of the rock mass forming the slope can also affect the style of failure of rock slopes. High quality, massive rock masses, are more likely to produce structurally-controlled deformations and landslides, whereas low quality, highly fractured rock masses can promote the occurrence of soil-like landslides, such as roto-translational landslides and rock slumps (Hungr et al., 2014; Agliardi et al., 2018; Stead et al., 2021). The characteristics of the intact rock (e.g., compressive, tensile, and shear strength, deformation behavior, fracture toughness) can also control the behavior and stability of rock slopes constituted by massive rock masses, with a poorly interconnected discontinuity network, in which the detachment of landslides is subordinate to the brittle propagation of fractures and failure of intact rock bridges (Havaej et al., 2014; Donati et al., 2019).

The stability of rock slopes is not a condition that remains unchanged with time. The prolonged action of exogenic processes (e.g., rainfall, seasonal water table changes, physical and chemical weathering) and endogenic processes (e.g., earthquakes) may progressively weaken a slope,

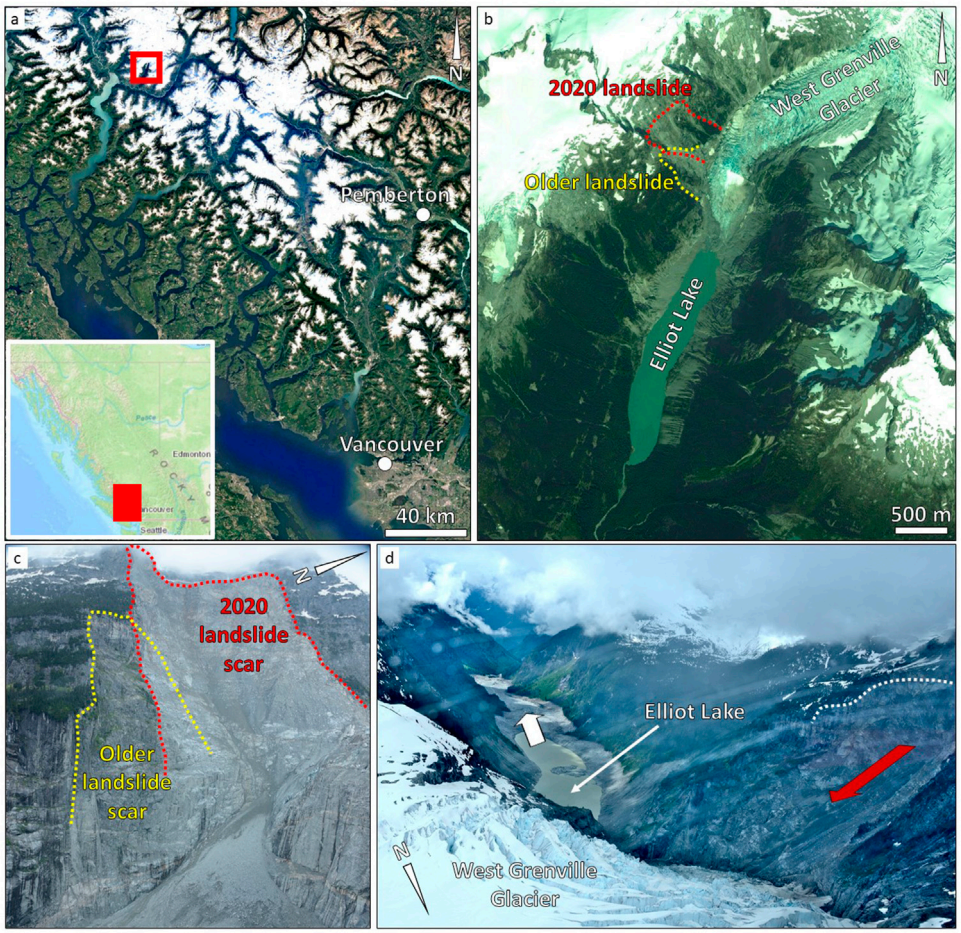

FIGURE 1 | Geographic overview of the study site. **(A)** location of the Elliot Creek landslide in southwestern British Columbia. **(B)** 2012 satellite imagery (Maxar Technologies imagery from Google Earth) showing the area affected by the landslide. The red, dashed line outlines the volume failed in 2020. The yellow, dashed line shows the inferred boundaries of the older landslide of unknown age. Note the Elliot Lake, at the valley bottom, formed after the retreat of the West Grenville Glacier. **(C)** oblique view of the landslide area, showing the boundary of the 2020 landslide and the inferred boundary of the older event (photo June 2021). **(D)** View from north of the Elliot Creek after the occurrence of the landslide, showing the effects of the landslide-generated wave on the valley slopes. The white, dashed curve outlines the landslide crest. The red and white arrows show the movement directions of the landslide volume and the landslide-generated wave, respectively (photo June 2021).

promoting progressive failure mechanisms (Whalley, 1974; Kemeny, 2005; Griffiths et al., 2012; Wolter et al., 2016). The erosive action of glaciers and rivers extended over long periods of time can also cause a progressive oversteepening of the slope, and promote landsliding due to stress concentrations and reduction of kinematic constraints (Larsen and Montgomery, 2012). Kinematic constraint is a condition that enhances the stability of a slope, through buttressing, lateral support, and lack of features along which displacement can occur. A reduction in kinematic constraint (i.e., an increase in kinematic freedom) can involve the development of rupture and sliding surfaces within the slope or a decrease in frontal or lateral support of a displacing volume, promoting rock mass deformation or displacement along pre-existing surfaces. In this regard, the detachment of landslides may abruptly modify the kinematic configuration and cause instability to propagate to previously stable parts of the slope (Donati et al., 2021a; Fullin et al., 2021).

In mountainous regions, glaciers also play a critical role in controlling the evolution and stability of valley slopes. Cycles of glacial advance and retreat are a well-known contributor to the instability in alpine regions (Böhme et al., 2015). Glaciers can result in erosion and slope oversteepening during phases of glacial advance and stability. Conversely, debuttressing with reduced lateral slope support and changes in slope kinematics (e.g., daylighting of geological structures resulting in an increased potential for landslide mobilization) occurs during intervals of retreat. Some notable examples of large-scale slope instability related to the oversteepening and subsequent reduction of lateral constraint and changes in kinematics include the Mitchell Creek landslide (Clayton et al., 2017), the Moosfluh landslide (Kos et al., 2016), and the Downie Slide (Donati et al., 2021c). To a lesser extent, subsequent phases of glacier advance and retreat, causing a progressive accumulation of damage within the rock slope due to the cyclic application of load, can promote the development of slope instabilities (Grämiger et al., 2017).

The 2020 Elliot Creek landslide is an interesting event because it resulted from the combination of a series of factors described above, namely the geomorphic evolution of the valley, the glacial history of the region, and the geological and structural configuration of the slope. In this paper, we first describe the structural, kinematic, and geomorphic characterization of the source area, to allow an interpretation of the failure mechanism, highlighting both the role of environmental and geological factors and processes in the evolution of the slope instability.

2 OVERVIEW OF THE ELLIOT CREEK LANDSLIDE

The landslide site is located approximately 150 km northwest of Vancouver, British Columbia (Canada) (**Figure 1A**) in the Pacific Ranges of the Coast Mountains (Holland, 1976). On 28 November 2020, an 18 million m^3 landslide detached from the western slope of Elliot Creek, in proximity of the retreating West Grenville Glacier tongue, and rapidly moved downslope, entering the Elliot Creek glacial lake, and producing a wave with a maximum runup of 114 m (Geertsema et al., 2022). The wave, with an estimated volume of 13.5 million m^3 of water, scoured the moraine at the southern end of the Elliot Lake and incorporated debris from the bed and lower slopes of Elliot Creek. The debris transported by the wave was then deposited at the intersection with the Southgate River, which flows from east to west 10 km south of the landslide site into the Bute Inlet. The Southgate River was temporarily dammed by the resulting debris fan, and the turbidity of the water current downstream of the debris dam was significantly increased for several weeks after the event (Geertsema et al., 2022).

A seismic signal was produced by the landslide, which was comparable to a M = 5 local earthquake. The landslide left a fresh scar on the rock slope, extending about 600 m downslope, between the ground elevations of 1870 and 1280 m a.s.l., and about 600 m along slope. The failure was preceded by progressive slope deformation, which eventually led to the detachment of the landslide. InSAR data analysis conducted on pre-failure datasets evidenced that the slope was deforming at an average rate of about 5.5 cm/y (measured along the satellite line-of-sight, LoS) between June 2018 and October 2020. Between June and October 2020, a cumulative LoS displacement of 15 cm was measured, corresponding to a 0.3 m/y LoS velocity over the summer 2020 (Geertsema et al., 2022).

The slope from which the 2020 Elliot Creek landslide detached was previously affected by another landslide of unknown age, but older than 1951 (Geertsema et al., 2022), which left a landslide scar that is visible in the pre-failure satellite and aerial imagery (**Figure 1B**). Prior to the 2020 event the older landslide scar appears to be relatively fresh and bounded by sharp, sub-vertical cliffs devoid of vegetation.

Lithologically, the landslide involved plutonic rocks, predominantly quartz diorite (Roddick and Woodsworth, 2006; Cui et al., 2017), Late Cretaceous to Early Tertiary age (about 100—50 million years BP), which was formed during the emplacement of the Coast Mountains batholith (Gehrels et al., 2009). The batholitic and volcanic complexes that exist along the western coast of British Columbia and Washington are linked to the subduction of oceanic crust under the North American Plate, which was accompanied by the progressive accretion of various terranes and microcontinents, and resulted in a significant crustal thickening (Monger et al., 1982; Colpron et al., 2007). The regional structural geology has a primary role in controlling the orientation of major valleys, which largely strike in a northwest-southeast direction, sub-parallel to the major thrust faults that characterize the southern part of the Coast Mountain Belt (Umhoefer and Miller, 1996).

The region has been significantly affected by the Cordilleran Ice Sheet, which shaped the morphology of valleys and slopes across the western part of North America, from the Alaska Range to the north, to the edge of the Cascade Range, in northern Washington and Montana, to the south. The Cordilleran Ice Sheet formed during the last Pleistocene glaciation (namely, the Fraser Glaciation, 25,000 years BP). At the time of maximum extension, it coalesced with the western edge of the Laurentide Ice Sheet (which covered the central and eastern Canada). At the peak of the Fraser glaciation, the Cordilleran Ice Sheet buried the alpine valleys in British Columbia below up to 2 km of glacier ice (Booth et al., 2003). The retreat of the ice sheet, which began with the Holocene interglacial, was completed by 11,000 years ago (Booth et al., 2003). However, the retreat of the Cordilleran Ice Sheet was noted to be diachronous. Evidence of glacial retreat and thinning even before the glacial maximum has been described (Menounos et al., 2017; Darvill et al., 2018), and parts of the coastal area were noted to be free of ice as early as 18,100 years BP (Darvill et al., 2018).

The behavior and displacement of the 2020 Elliot Creek slide prior, during, and after the slope detachment, as well as the impacts produced along the Elliot Creek have been summarily described in the work by Geertsema et al. (2022). However, the environmental, structural, geomorphic factors that controlled the detachment of the 2020 Elliot Creek landslide have until now not been studied. The importance of slope kinematics, which is dependent on interaction between slope morphology and the orientation, persistence, and spacing of structural discontinuities has not been analyzed and discussed in detail. The impact of the detachment of the older landslide block on the stability of the slope and the possible progressive failure mechanism have not been investigated. Finally, the role of on-going global warming on stability has yet to be addressed in detail. Research by Menounos et al. (2019) and Hugonnet et al. (2021) revealed that recent changes in climate caused glaciers to experience strong mass loss throughout Western North America and in the Coast Mountains. Based on these findings, Geertsema et al. (2022) posit that retreat of the West Grenville Glacier played a role in destabilizing the slope that failed above Elliot Creek. However, it remains uncertain the degree to which glacier thinning contributed to the instability. Therefore, the objective of this paper is twofold: first, to outline the role of geological structures at various scales (from regional- to slope-scale), and second, to investigate how the older landslide and the retreat of the West Grenville Glacier contributed to the long-term evolution of slope kinematics and stability that ultimately led to the 2020 landslide. First, we

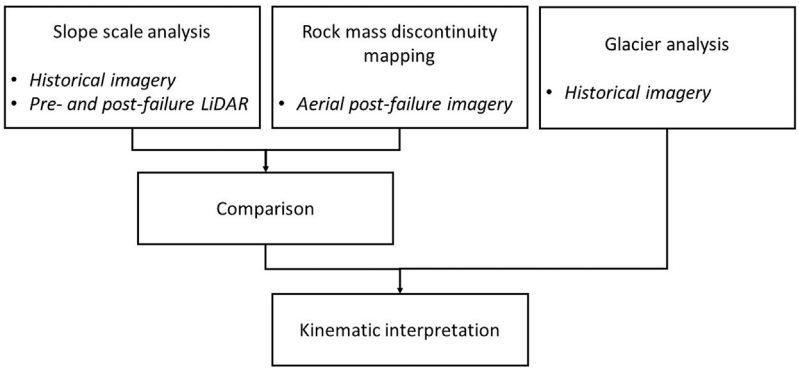

FIGURE 2 | Flowchart showing the types of input datasets used in the various stages of the landslide characterization.

use pre- and post-failure remote sensing datasets to characterize the slope, identifying structural and geomorphic features that combined to define the slope kinematics. Then, we use historical imagery to assess the change in glacier extent and surface elevation. Finally, we combinedly analyze the results of the analyses, to allow the reconstruction of the geomorphic history of the slope, the interpretation of the failure mechanism, and the potential role of glacier retreat and thinning on the evolution of the landslide.

3 WORKFLOW AND METHODS

3.1 Workflow

Our research employed a hierarchical approach to investigate the slope at progressively smaller scales. First, we performed a slope-scale characterization of the landslide area, using pre- and post-failure digital elevation models (DEMs) derived from airborne LiDAR (light detection and ranging) surveys, as well as historical aerial imagery. The pre- and post-failure datasets are characterized by a resolution of 3 and 1 m, respectively. Close-up photographs were then used to create a virtual outcrop of a sector of the rupture surface, to characterize the rock mass in greater detail. The results from the analyses at these various scales were combined and used to reconstruct the kinematic configuration of the slope (as well as its variation over time) and assess its role in the stability and geomorphic evolution of the rock slope (**Figure 2**). The following paragraphs provide a more detailed summary of the datasets employed, as well as the objectives, and the nature of the results expected from each analysis.

3.2 Slope Scale Characterization

The slope scale analysis of the Elliot Creek landslide source area was focused on the characterization of the morphology and structural characteristics of the ground surface before and after the event. Such an analysis was conducted using a pre-failure airborne LiDAR dataset (collected on 11 October 2019 using a Riegl Q780 full waveform scanner mounted on a fixed wing aircraft) and a post-failure dataset (collected on 23 December 2020, using the same instrument mounted on a helicopter). The Riegl Q780 was coupled with an Applanix Pos910 AV Inertial Measurement Unit/Global Navigation Satellite System (IMU/GNSS, Pelto et al., 2019).

Hillshade, slope, and aspect maps were derived from the pre- and post-failure DEMs. The pre-failure maps were assessed to identify indicators of slope instability, particularly tension cracks along the boundaries of the landslide body. The post-failure dataset was then used to perform a lineament analysis in a GIS environment, using a methodology similar to that presented in (Donati et al., 2021b). Lineaments mapped at this site are represented by linear geomorphic features, such as scarps and anti-slope scarps, cracks and fractures, gullies and stream incisions. Geometric characteristics of such elements, including length, trend, and location, are typically controlled by geological structures at various scales (e.g., faults, joints), and can therefore provide information on the structural configuration of the mapped rock slope. The orientation of the mapped lineaments, plotted in rosette diagrams, were used to identify the trend of major lineament sets. These were then compared with regional-scale geomorphic and structural features (e.g., valley, crest, and coastline trends) observed in satellite imagery, as well as outcrop scale structural features (e.g., joints, faults) mapped in virtual outcrops (see. **section 3.3**).

Profiles were traced downslope and across the landslide area, within both the pre- and post-failure datasets, to investigate the relation between the geomorphic characteristics of the slope and the structural and kinematic configuration of the rupture surface.

3.3 Rock Mass Discontinuity Mapping

The outcrop scale analysis focused on characterization of the discontinuities within the rock mass involved in the slope failure. A 3D virtual outcrop was developed through a Structure-from-Motion (SfM) approach, using multiple oblique photographs taken from a helicopter. Photographs were collected with a 36.3 MPixel Nikon D800 DSLR camera, equipped with a f=28 mm focal length optical lens. The 3D model was created using the software Metashape 1.8 (Agisoft LLC, 2021), whereas the discontinuity mapping was performed using the software CloudCompare 2.11 (CloudCompare, 2020), which allows the

orientation of structural discontinuities to be determined from planes and traces visible across the virtual outcrop.

The discontinuity data was then plotted in stereonets, to identify the major discontinuity sets. Rosette plots were also produced to allow comparison with the slope scale analysis, and to investigate the potential role of rock mass discontinuities on the landslide morphology and boundaries.

3.4 Glacier Retreat Analysis

To evaluate the relationship between slope stability evolution and the evolution of the West Grenville Glacier, we computed a DEM from two air photos acquired on 23 July 1965 by the government of British Columbia using the open-source photogrammetry software MicMac (Rupnik et al., 2017; see also https://micmac.ensg.eu/). Before processing, the grayscale images were enhanced with a contrast-limited adaptive histogram equalization (CLAHE), and salt-and-pepper noise minimized using a 3 × 3 pixel median filter. This improved contrast for snow and ice pixels.

After computing tie-points between images, a relative orientation was generated and then transformed into an absolute reference system with ground control points (GCPs). Using the 2019 LiDAR DEM (3 m resolution) as reference, we collected 45 GCPs from prominent features (e.g., large boulders) in stable terrain, and used these to transform the camera locations into absolute space. A bundle adjustment run with GCPs was used to refine the 3D geometry of the absolute orientation. Finally, a DEM and orthophoto were computed at 5 m resolution using a semi-global image-matching algorithm (Rupnik et al., 2017).

Before calculating surface elevation change on the West Grenville Glacier, the 1965 and 2019 DEMs were co-registered over stable terrain, using the approach of Nuth and Kääb (2011). Subsequently, an elevation change (*dh*) raster was computed by differencing the 1965 photogrammetric DEM and the 2019 LiDAR DEM on a pixel-by-pixel basis. Using a correlation mask generated by MicMac during the image-matching, low confidence pixels (i.e., pixels with correlation values below 65, a threshold below which, based on visual inspection of the DEM and orthophoto, artifacts occur; see Denzinger et al., 2021) were excluded from the *dh* raster. The excluded pixels were filled hypsometrically (see McNabb et al., 2019), using the median *dh* value of 10 m wide elevation bins.

Two profiles, traced through the 1965 photogrammetric model and the 2019 LiDAR DEM, were also extracted in a GIS environment to investigate the potential impacts of glacier retreat and thinning on the geomorphic evolution of the investigated slope.

3.5 Kinematic Interpretation

Combined interpretation of the results from the slope scale characterization, outcrop scale mapping, and glacial retreat analysis were used to provide an interpretation of the factors that controlled the kinematic configuration of the landslide and, in turn, the overall stability and evolution of the rock slope.

A block model of the slope was produced, to highlight the structures that, at various scales, controlled the size and location of the landslide. The role of the glacier and its retreat on the stability of the slope was inferred, considering both the location, over time, of its terminus, as well as the changes in ice thickness in correspondence of the slide area. The role of the older landslide event on the long-term stability of the slope was addressed, with regard to the impacts on the kinematic constraint of the slope, and its role on the development of the 2020 landslide.

Based on the analyses presented in this paper, in addition to the findings from previous studies (e.g., pre-failure slope deformation), a conceptual model was presented, which describes the geomorphic and environmental changes that occurred in the Elliot Creek valley since the end of the Fraser Glaciation.

4 RESULTS

4.1 Slope Scale Characterization

The analysis of the hillshade, aspect, and slope maps derived from the pre- and post-failure datasets allows for the analysis of geomorphic features within the slope where the Elliot Creek landslide occurred. A side-by-side comparison of such datasets showed that, to the northeast, the landslide volume was laterally bounded by a zone of stream incision, which 1) may have facilitated the detachment by providing kinematic freedom to the side of the landslide, or 2) may have resulted from the progressive deformation of the slope recognized in the InSAR datasets described in (Geertsema et al., 2022). The southwestern lateral boundary of the landslide body was kinematically free, following the removal of part of the slope during the older landslide (**Figure 3A**). In the upper part of the landslide area, along the incipient crown, the pre-failure dataset displays a relatively smooth ground surface, with no obvious slope damage features, particularly in the central part of the incipient crown. This area appears to be largely blanketed by colluvium in pre-failure, high-resolution, aerial photographs. However, open fractures can frequently be observed at both sides of the incipient landslide crown, including beyond the landslide area (**Figure 3C**). Moreover, a scarp located at the intersection between the lateral and upper boundaries, but outside of the landslide area, appears to have propagated westward forming part of the upper release surface (**Figures 3B,C**). The upper landslide boundary is characterized by a stepped morphology, as it is formed by two linear features parallel to the valley, connected by an orthogonal fracture.

While the central and upper part of the slope dips 45°–60°, the lower slope is characterized by an increase in steepness (more than 80°), likely resulting from the long-term erosion of the West Grenville Glacier (**Figure 3D**). Here, like in the upper landslide, the rupture surfaces of both the older and the 2020 rock slides also display stepped morphologies which are particularly visible in the steeper parts of the rupture surface. The identified steps are characterized by varying length, generally 50–150 m, and height, up to 30–40 m. Two orthogonal sets of steps can be observed (**Figure 3D**). One set is formed by steps dipping in an east- to northeast direction, as observed both in the slope map and in profile 4 traced across the slope, orthogonally to the steps

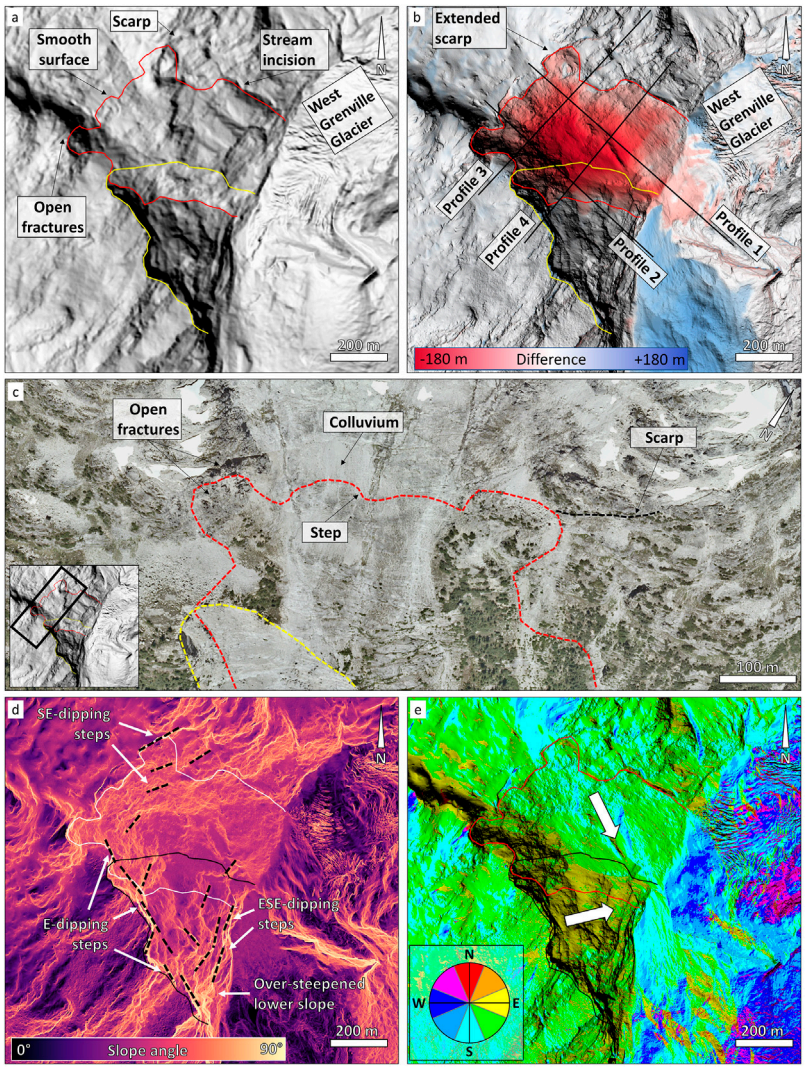

FIGURE 3 | Comparison of pre- and post-failure datasets. **(A)** Pre-failure hillshade map. The yellow and red curves outline the surface area of the old and the 2020 landslide event, respectively. Note the void left by the older landslide to the south, and the stream incision that marks the opposite side of the landslide volume. **(B)** Post-failure hillshade map, overlayed with the difference with the pre-failure LiDAR dataset. Red and blue shades represent elevation loss and gain, respectively. Profiles 1–4 are displayed in **Figure 5** and discussed in the text. **(C)** Detail of a 2006 aerial photo showing the upper landslide area. Note the stepped, incipient rupture surface (red dashed line) that intersects areas with open fractures and colluvium cover. The scarp extended during the 2020 landslide is also highlighted. **(D)** Post-failure slope map, showing the steepening of the ground surface in the lower slope, and the varied dipping of the main step sets. Note the E-dipping steps that control and partly form the southern boundary of the older landslide area. **(E)** Post-failure aspect map. Note the older landslide area, characterized by an overall ENE dip direction, and the scar of the 2020 landslide event, for the most part dipping to the SE.

(**Figure 4**). These steps appear to have laterally constrained the old landslide displacement and volume. The other set of steps dip to the east-southeast. Across most of the basal rupture surface of the recent landslide the easterly dipping topographic steps are not recognizable. However, southeasterly dipping steps can be observed in the upper part and lower part of the slope, where slope angle is greater (**Figures 3C**, **4A**). In the central part of the slope, no stepped morphology can be discerned, due to both the lower slope angle and landslide debris.

Profiles 1 and 2 (**Figures 4A,B**), traced downslope in the pre- and post-failure datasets, and profiles 3 and 4 (**Figures 4C,D**), traced across the slope, clearly show the elevation change produced by the 2020 event, which is up to 180 m in the upper slope, towards the northern boundary of the landslide. The pre-failure profiles also highlight the impact of the older landslide on the slope morphology. The estimated original slope profile can be inferred by considering the upslope topographic surface, the void volume produced by the old landslide and the glacially over-steepened lower part of the slope. This old landslide most likely moved along a major structurally-controlled plane with average orientation 40°/120° (dip/dip dir.). The same structure appears to have formed part of the rupture surface of the 2020 landslide (**Figures 4A,D**), suggesting that the two events were at least partly controlled by the same structural

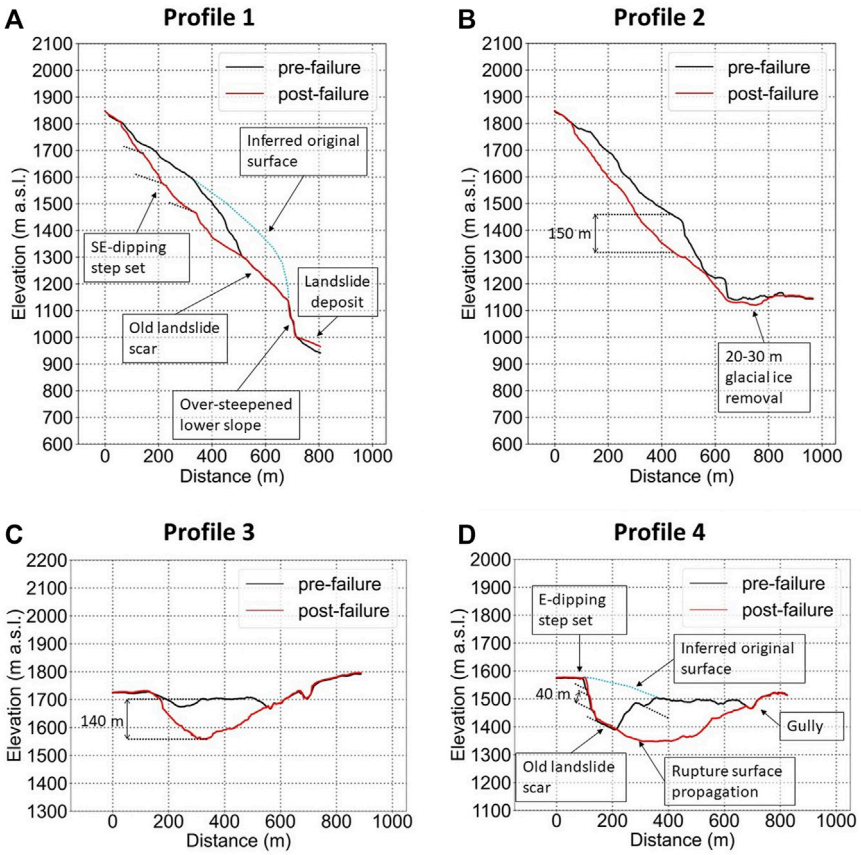

FIGURE 4 | Overview of the profile analysis. In **(A)** (profile 1), note the steps in the upper, post-failure slope surface, and the inferred profile before the old landslide. In **(B,C)** (profiles 2 and 3) the thickness of the landslide and the glacier ice removal are displayed. In **(D)** (profiles 4) the stepped surface forming the boundaries of the older landslide in the pre-failure slope topography is shown.

features, including the 3D stepped morphology that characterizes the rupture surface of both events.

The location of the landslide appears to correlate with structural geomorphic features that may have played a role in the long-term slope stability evolution of the area (**Figure 5**). Just north of the landslide, Elliot Creek displays a 40° change in trend from a southwest direction to a south-southwest direction (**Figure 5B**). This change in valley direction is also marked by a prominent, 300 m-high, geomorphic step, orthogonal to the valley, that divides the lower, south-southwest trending valley, below an elevation of 730 m a.s.l., from the higher, southwest trending valley, above 1140 m a.s.l. (**Figure 5C**).

The lineament analysis performed using the post-failure airborne LiDAR dataset allowed 238 unique linear features to be identified and mapped (**Figure 6A**). Rosette diagrams, created by plotting the trend of the mapped linear features, allowed two prominent lineament trends to be identified, L1 and L2, characterized by approximately orthogonal directions. Lineaments ascribed to L1 trend in a northwesterly direction (300°–360°), whereas L2 trend, on average, in a northeasterly direction (20°–90°). However, a bi-modal distribution is observed for L2, which feature abundant lineaments with a 45° trend (referred to as L2a in **Figure 6B**) and a 65° trend (referred to as L2b in **Figure 6B**). Additional Rosette diagrams were produced, in which lineaments were filtered by length, however, no significant difference was observed by only plotting features longer than 50 and 100 m.

The identified lineament trends appear to control the orientation of the different sets of steps observed across the rupture surface. The easterly dipping geomorphic steps observed along the western part of the slope (i.e., the old landslide scar) are controlled by L1 lineaments. The effect of the bi-modal distribution of L2 lineaments can be recognized in the varying orientation of the geomorphic steps between the eastern part of the slope (controlled by L2a lineaments) and the western part (controlled by L2b lineaments).

The orientation of L1 and L2 also mimic the orientation of regional scale physiographic features in and around the Homathko Icefield plateau (**Figure 6C**). Notably, the Homathko River valley follows the western boundary of the icefield plateau, flowing in a southwesterly direction, similar to the L2a lineament trend, northwest of the icefield, before entering Bute Inlet flowing in a southeastern direction, similar to the L1 trend. Various other minor valleys trend in a northwestern

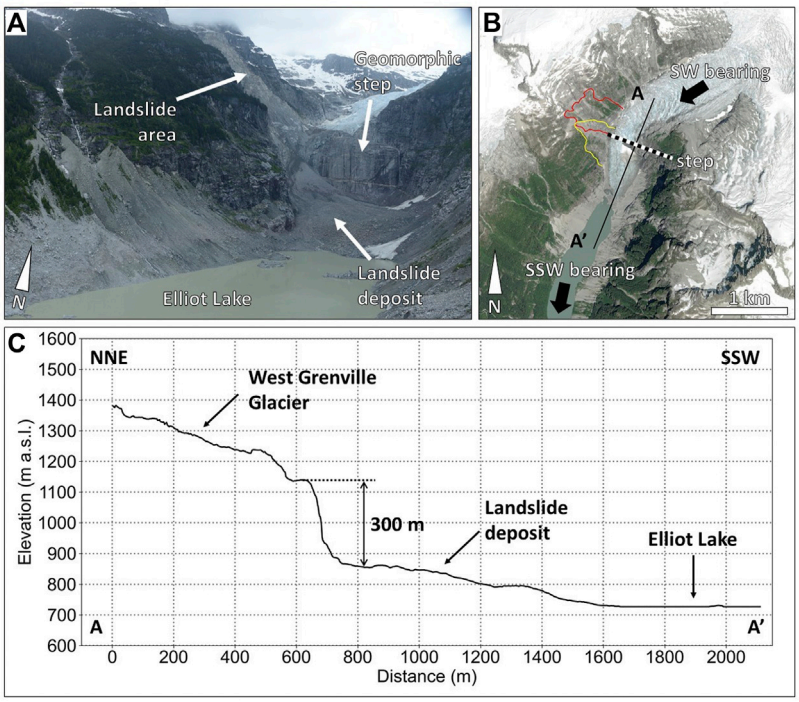

FIGURE 5 | Overview of the geomorphic configuration of the Elliot Creek near the landslide area. **(A)** oblique view of the Elliot Creek, looking north, showing the geomorphic step on which West Grenville Glacier is located (photo June 2021). **(B)** satellite view (ESRI World Imagery Map) of the landslide area prior to the failure. The varying trend of the Elliot Creek above and below the step is highlighted. The boundaries of the old and the 2020 landslides are marked by the yellow and red curve, respectively. The profile along the A-A′ segment is shown in **(C)**. **(C)** Profile along A-A′ in **(B)**. The geomorphic step roughly occurs at the interface between the rupture surfaces of the old and 2020 landslides.

direction, similar to the L2a and L2b lineaments. Elliot Creek above the geomorphic step shown in **Figure 5** trends in a direction similar to L2b. However, the trend of several prominent physiographic features that can be observed at a regional scale, such as the Southgate River valley and its tributaries, including the lower Elliot Creek, is skewed 20–30° counterclockwise compared to the average trend of the L1 and L2a-b lineament trends, highlighting the complex structural geological setting of the study area.

4.2 Rock Mass Discontinuity Mapping

The rock mass characterization, performed on the 3D model derived from the helicopter-SfM survey, allowed 120 discontinuities to be identified and mapped (**Figure 7**). The smallest mapped feature is characterized by an estimated persistence of 6 m.

The poles of the mapped discontinuities were plotted in a stereonet, allowing three major discontinuity sets (D1-D3) and three minor sets (D4-D6) to be identified. The set D1 is characterized by an orientation of 41°/123° (dip/dip dir.), roughly parallel to the trend of Elliot Creek. The average persistence of the D1 discontinuities is 83 m, which is largely a result of the mapping of the elongated, across slope steps characterizing the basal rupture surface (**Figures 7A,B**). The other major discontinuity sets, D2 and D3, are sub-vertical and sub-parallel to each other, and display an average orientation of 88°/063° and 88°/270° (**Figure 7B**) and have an average persistence of 92 and 65 m, respectively. The minor discontinuity sets D4, D5, and D6 display orientations of 80°/306°, 79°/157°, and 47°/210°, respectively.

The orientation data of rock mass discontinuities with a dip angle greater than 60° was displayed in a Rosette diagram and compared with that resulting from the slope-scale lineament analysis (**Figure 7C**). We note a close agreement between the sets D2 and, to a lesser extent, D3, and trend L1. We also note a good agreement between the combination of sets D4 and D5 and trend L2a. A limited number of mapped discontinuities display an orientation similar to L2b.

4.3 Glacier Retreat Analysis

By differencing the 2019 airborne LiDAR DEM and 1965 SfM-derived DEM we were able to evaluate the change in ice surface elevation of the West Grenville Glacier, as well as the retreat of the glacier terminus that occurred over the 54-year period (**Figure 8**). The reduction in glacier surface elevation is particularly significant downstream of the 300-m-high geomorphic step that crosses the valley. In some locations, the ice surface thinned by 175 m (**Figure 8A**). Upstream the step, the amount of surface lowering varies between 30 and 60 m, with the highest values observed in proximity of the geomorphic step. Overall, ice thinning rarely exceeded 50 m, and progressively decreased towards the accumulation area of the West Grenville Glacier.

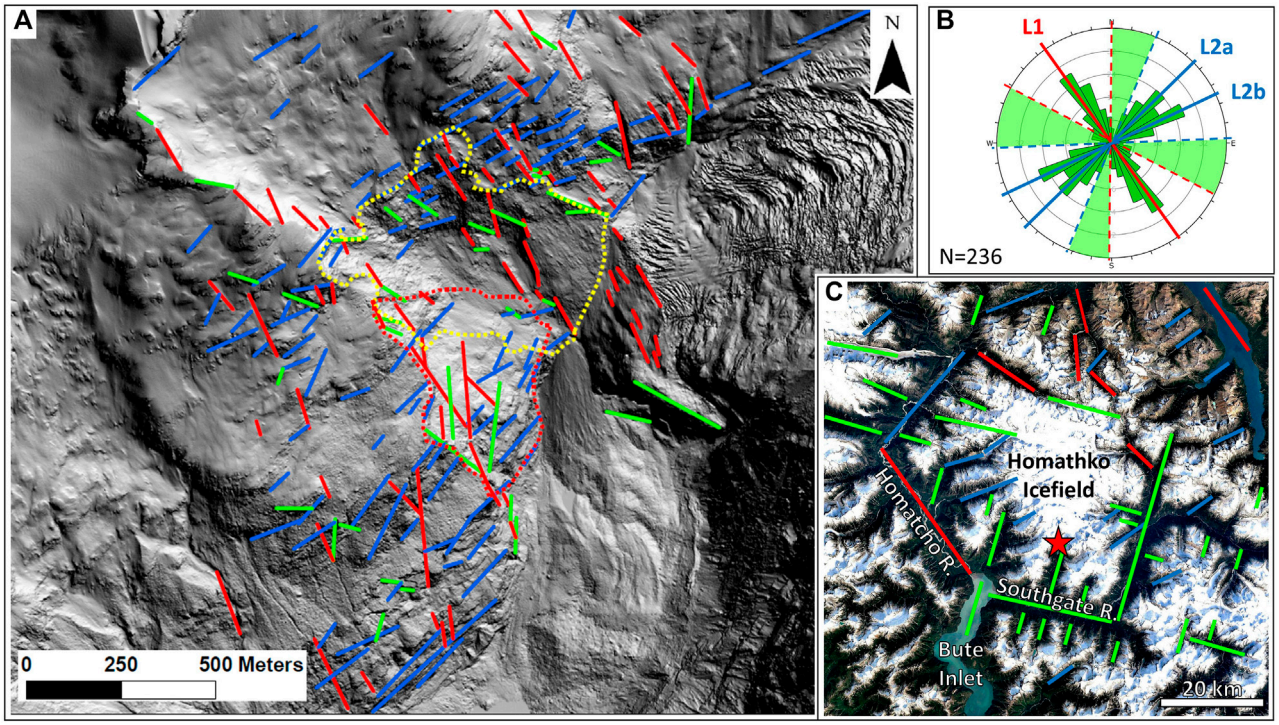

FIGURE 6 | Lineament analysis summary. **(A)** lineament map of the slope affected by the 2020 landslide, overlayed on the post-failure hillshade map. Mapped lineaments are color-coded based on the trend shown in **(B)**. **(B)** Rosette diagram showing the trends of the major observed lineaments. Green zones in the diagram identify the lineaments that cannot be ascribed to a specific trend (green lines in **(A,C)**. **(C)** Regional map showing the similarity between lineament trends and geomorphic features (e.g., river valleys). Red star indicates the location of the landslide area towards the head of Elliot Creek.

We evaluate the potential effects of glacial retreat and thinning on slope stability across two transects positioned over the landslide area. We suggest that below the geomorphic step, the glacier thinning that occurred since 1965 did not affect the stability of the rock slope, as the elevation of ice surface in 1965 was already below the basal rupture surface of both the old and 2020 landslides (**Figure 8B**). However, above the geomorphic step (i.e., the northern part of the landslide area), the glacial retreat since 1965 likely had a more significant impact on slope stability. The 1965 ice surface was higher than the daylighting rupture surface, and thus the glacier was likely providing some support to the rock slope. In 2019, most of the supporting capability of the West Grenville Glacier had vanished due to thinning, and the rapid displacement of the landslide became possible.

Other than the amount of glacier thinning, the investigated profiles also display a prominent increase in slope angle (i.e., a slope break) at elevations of 1350 m and 1450 m a.s.l., below and above the geomorphic step across the valley, respectively, which possibly mark the glacial maximum that occurred during the Little Ice Age (LIA).

5 DISCUSSION

The Elliot Creek slide is bounded by lineaments with orientation similar to regional-scale physiographic features, such as river valleys, as well as smaller scale rock mass discontinuities mapped across the landslide rupture surface. Such a geomorphic configuration indicates a significant role of structural geology on the location, size, and evolution of the landslide. Importantly, the change in valley orientation (**Figure 5B**), controlled by regional geological structures, likely resulted in a significantly more damaged rock mass (e.g., increased fracture intensity and decreased rock mass quality) and, in turn, an enhanced susceptibility to landsliding.

In order to investigate the role of structural features in the landslide at various scales, two separate kinematic analyses, conducted using data from the slope scale characterization and rock mass discontinuity mapping (**Figure 9**), provided corroborative evidence for wedge sliding along discontinuity set D1, which strikes parallel to the valley direction, and is characterized by a dip angle lower than the slope. The close similarity in their orientation suggests that the structurally controlled surface, shared between the rupture surfaces of the old and the 2020 landslide, is formed by interconnected, persistent D1 discontinuities. Slope-scale kinematic release is provided by the major geological structures resulting in lineaments L1 and L2 (preliminarily assumed as vertical in the kinematic analyses), which control and constitute lateral and rear release surfaces for the landslide (**Figure 9A**). Note that in this discussion on slope kinematics, we use L1 and L2 to refer to the geological structures that intersect the slope surface forming these lineament sets. Displacement occurred along the intersection of

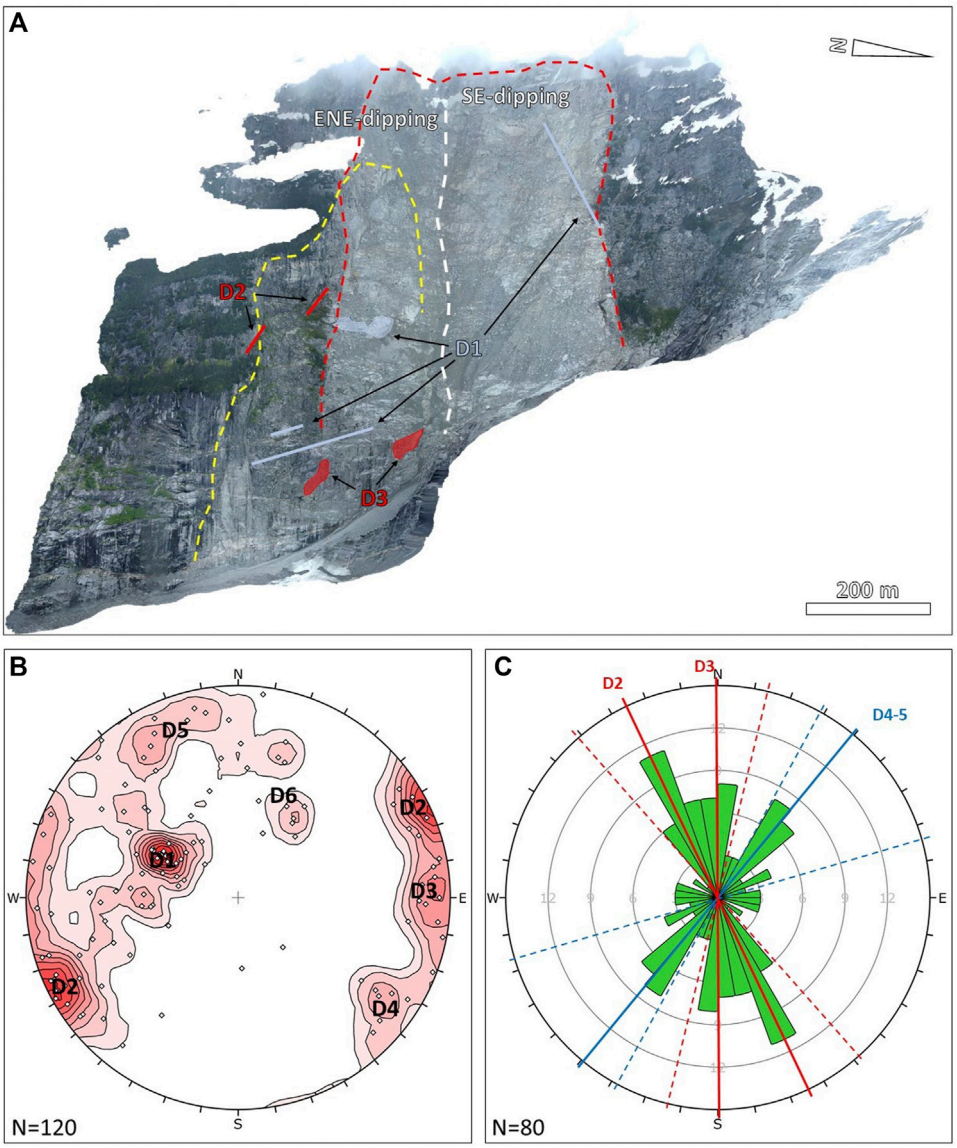

FIGURE 7 | Summary of the rock mass discontinuity mapping results. **(A)** orthorectified image of the landslide area, showing sample features of the major discontinuity sets D1-D3. The yellow and red dashed curves outline the boundaries of the pre-1950 and the 2020 landslides. The white dashed line marks the change in average slope direction (see **Figure 3E**) **(B)** oblique view of the landslide area, showing samples of the major discontinuity sets. **(C)** lower hemisphere, equal angle stereonet showing the poles of the mapped discontinuities. **(C)** Rosette diagram displaying the trend of mapped discontinuities with dip angle greater than 60°.

D1 and L1, with the latter largely acting as a lateral release. The morphology of the simulated rock wedge is very similar to the landslide scar produced by the 2020 event (**Figures 9A,B**). Similar results were derived from the kinematic analysis based on rock mass discontinuity mapping, with some limited differences in the orientation of the rear release surface, which stem from the different orientation between L2 and discontinuity set D3. SWedge (Rocscience, 2016) was used to visualize the morphology of the conceptual rock wedges outlined by the kinematic analyses (**Figures 9B,C**). Because of the comparable structural configuration, it is likely that the older landslide involved a similar failure mechanism.

From a geomorphic perspective, the 2020 Elliot Creek landslide may have been affected by both the occurrence of the older landslide, and the progressive retreat, and decrease in glacier thickness. The occurrence of landslides is known to play a potentially significant role in the long-term evolution of slopes, particularly for structurally controlled slope failures in rock. The detachment of a landslide may enhance the kinematic freedom of a slope, particularly if it involves the removal of a key block (Goodman and Shi, 1985). When this happens, the instability may propagate to previously stable parts of the slope, and new detachments may occur either through the same kinematic failure mechanism (e.g., planar sliding), or through a different

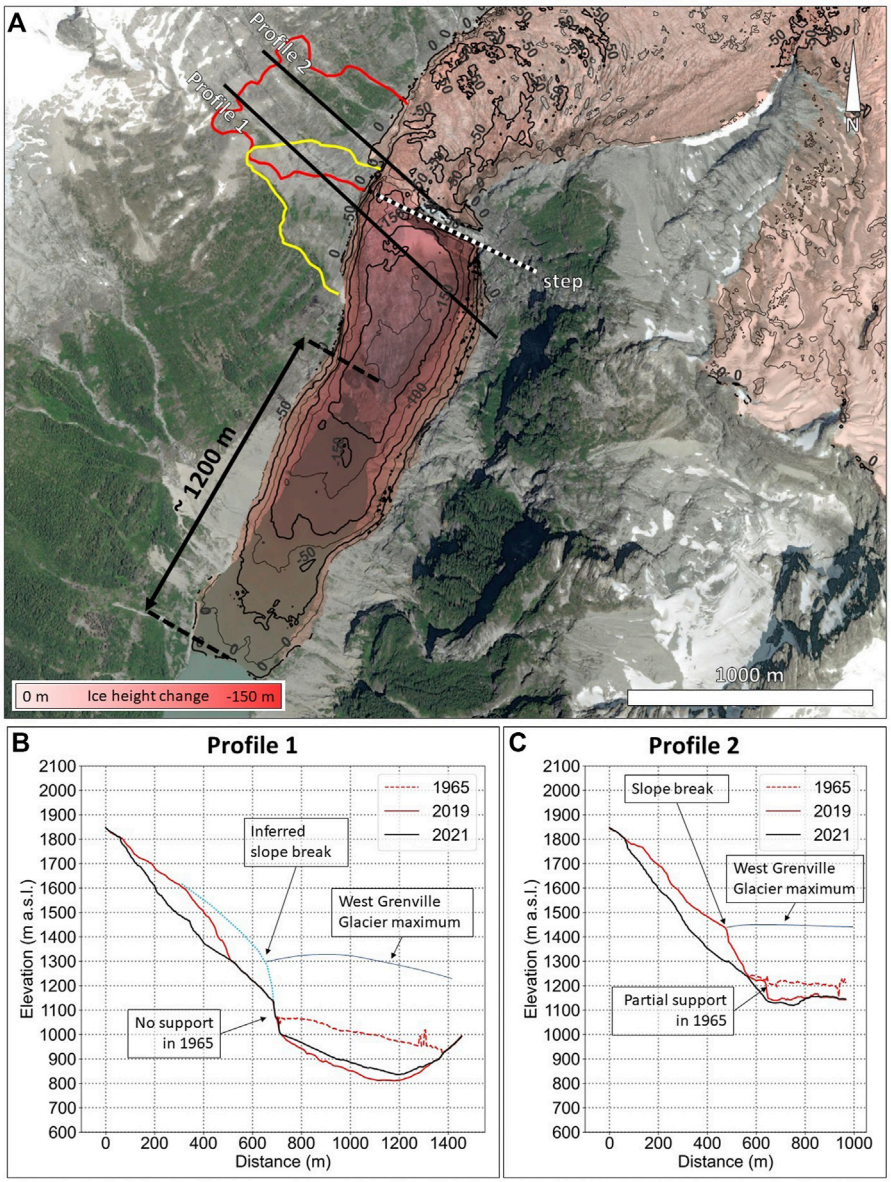

FIGURE 8 | Summary of glacier change analysis. **(A)** map of the computed change in ice surface elevation between 1965 and 2019. The total retreat of the glacier terminus has been estimated at 1200 m. The maximum change in ice elevation of 175 m occurs immediately downstream of the geomorphic step that crosses the valley near the landslide area. Traces of profiles 1 and 2, plotted in **(B,C)**, are shown. The yellow and red curves outline the old and 2020 landslide events, respectively. **(B,C)**: profiles showing the change in slope and ice surface elevation from 1965 to 2021. Note the lack of support provided by the glacier in 1965 along profile 1, and the limited support provided to the slope in profile 2 in the same year. The slope break (inferred in profile 1) are hypothesized to represent the maximum height of the West Grenville Glacier.

mechanism, which only became feasible after the removal of the key block. Significant examples include the Hope Slide in British Columbia, Canada (Donati et al., 2021c) and the Randa landslides in Switzerland (Eberhardt et al., 2004). At Randa, two subsequent landslides involved the rock slope in April and May 1991. The first slope failure was the ultimate effect of damage accumulation due to the glacial history of the valley and stress concentrations related to the slope morphology (Leith et al., 2014). The second landslide was driven by the change in kinematic configuration, as the volume removed during the first event represented a key block for the slope. In the case of the Elliot Creek landslide, the empty volume left by the older landslide likely led to the occurrence of the 2020 event, through a decrease in lateral support within the lower part of the rock slope and the initiation of a progressive failure mechanism, following stress concentration along the incipient rupture surface due to slope steepening. Such process has been described by several authors as an important cause of landslides in alpine regions (e.g., Riva et al., 2018).

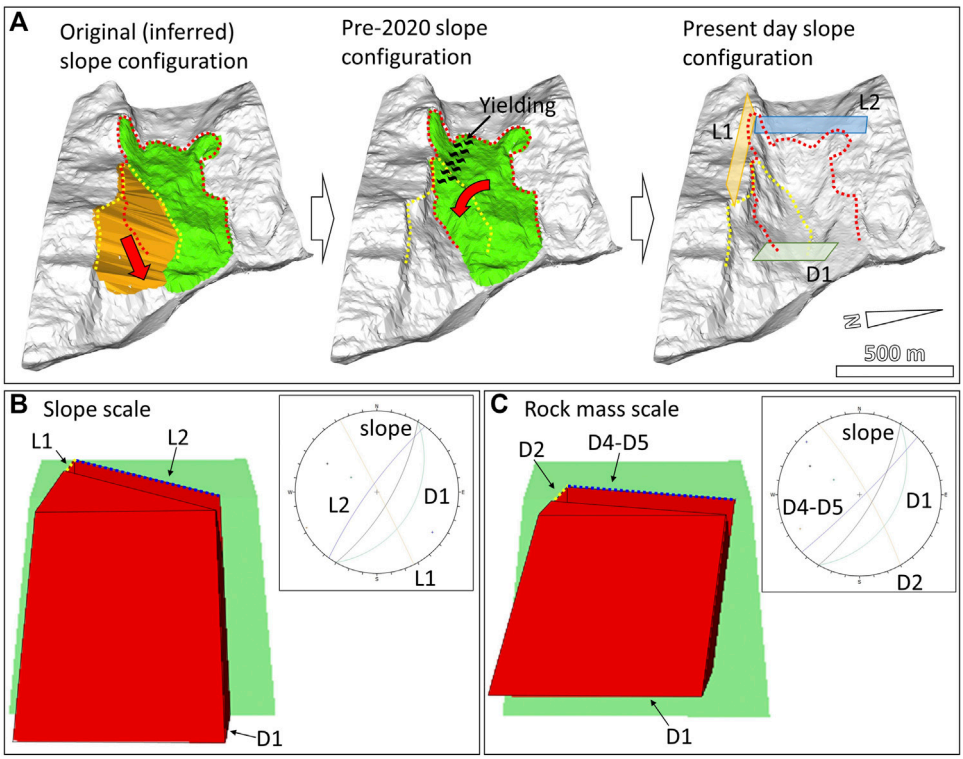

FIGURE 9 | Summary of kinematic analysis of the rock slope. **(A)** evolutionary block model of the landslide. Yellow and red dotted curves outline the boundaries of the old and 2020 landslide event, respectively. Red arrows represent the inferred displacement direction of the landslides. The orange block represents the older, undated landslide that affected the slope. Block morphology was reconstructed by interpolating a surface across the edges of the old landslide scar. The green block represents the volume detached during the 2020 event. Block morphology was built using the pre-failure LiDAR dataset. Note the inferred torsional component inferred for the block, produced by the asymmetric kinematic constraint in the lower slope, and the inferred area of rock mass yielding kinematically required for the movement to occur. The present-day slope configuration conceptually displays the slope-scale structures that controlled the 2020 landslide and were included in the slope scale kinematic analysis shown in **(B)**. **(B)** results from the slope-scale SWedge analyses using D1 as basal surface and lineaments L1 and L2 as lateral and rear release surfaces, respectively. **(C)** results from the rock mass scale SWedge analyses using D1 as basal surface and discontinuity sets D2, and D4 and D5 as lateral and rear release surfaces, respectively. The average, pre-2020 failure slope orientation was used for the model surface.

The progressive retreat of the West Grenville Glacier from the valley floor (about 1,200 m over 54 years) as well as the reduction in thickness also may have played a significant role in the slope evolution. At the time of failure, the tongue of the West Grenville Glacier was 300 m downstream the landslide boundary. However, the elevation of the glacier surface was 1000 m a.s.l. in the southern part of the landslide area (below the 300-m-high geomorphic step across the valley), and about 1150 m a.s.l. in the northern part (i.e., above the step). Therefore, the thickness of the glacier ice potentially opposing the landslide movement at the time of failure was limited spatially to the northern part of the landslide. Here, the magnitude of lateral support was also limited, due to the low elevation of the glacier ice above the toe of the landslide. The historic analysis showed that in 1965 the ice reached elevations of 1170 m and 1230 m a.s.l. at the landslide area above and below the step, respectively, suggesting that the West Grenville glacier ice was providing a greater support to the northern part of the landslide area. Considerations on the long-term correlations between glacier and slope stability can be tentatively derived from the analysis of the slope map (**Figure 3D**) and the profiles traced along the slope (**Figures 4A,B**). These datasets show that a prominent slope break occurs between the elevation of about 1350 m and 1450 m a.s.l., in the southern and northern parts the landslide area (i.e., above and below the geomorphic step crossing the valley), respectively. Note that the elevation of the slope break is estimated, in the southern part, based on the inferred topography prior to the older landslide. Such a slope break possibly marks the elevation of the glacier ice during the LIA. In this hypothesis, at that time the glacier ice may have provided a significant lateral support to the slope across the whole landslide area, largely preventing displacements as a result of kinematic constraint. Conversely, during the glacial retreat, the progressive reduction of glacier ice elevation in front of the landslide area caused a significant decrease in lateral support and kinematic constraint, ultimately allowing the daylighting of the structurally controlled surface along which both the older and the 2020 landslides displaced. Such an interpretation entails processes very similar to those that have been described for several other alpine sites (e.g., Holm et al., 2004; Kos et al., 2016). However, additional data (e.g., elevation of LIA moraine along the Elliot Creek) should be collected and investigated to support the hypothesis. It is also important to note

that even if the presence of glacier ice in front of a slope can prevent its rapid displacement, slow deformations, and thus the progressive accumulation of slope damage can occur (McColl et al., 2010). In other words, slope weakening and strength reduction can affect a rock slope buttressed by a glacier, promoting the occurrence of rapid landslides as glacier retreats.

In addition to their contribution to a progressive failure mechanism, the combined effect of the older landslide and glacial ice partly occupying the valley floor (particularly in the northern part of the landslide) may have caused the development of a complex kinematic failure mechanism. The presence of the empty volume along the southern boundary of the landslide undoubtedly defined a condition of kinematic freedom, which effectively enhances the mobilization of landslides. Such a hypothesis is supported by the observation of the structurally controlled surface that constituted the basal rupture surfaces of both the old landslide event and the 2020 landslide, which was, therefore, partly unsupported. The role of the lateral support of the glacier in the short term is less clear. The comparison between the pre- and post-failure airborne LiDAR datasets evidenced that a limited volume of glacial ice at the foot of the slope was removed during the failure, in the northern part of the landslide area. Presently, however, it is unclear whether the West Grenville glacier was still providing a relevant lateral support to the landslide at the time of failure, thus outlining a condition of partial kinematic constraint in the lower slope. From a kinematic perspective, an asymmetric distribution of lateral support at the base of the slope may have resulted in the development of a torsional component affecting the displacement of the landslide (**Figure 9A**), as conceptually described in Goodman (1995) and Hungr and Amann (2011). It is worth noting that such a rotational movement of the landslide body in the first stage of the displacement would have required internal rock mass deformation and yielding to overcome the lateral constraint provided by the slope to the upper part of the landslide (**Figure 9A**). Preliminary InSAR analyses described in Geertsema et al. (2022) show that pre-failure slope deformation was largely concentrated in the area near the older landslide scar, with highest magnitudes within the central and upper parts of the slope. Such a slope displacement distribution seemingly supports the hypothesis of a varying kinematic constraint along the lower slope and, possibly, the development of a torsional displacement component prior to the failure.

5.1 Implications for Numerical Modelling

Future investigations to quantitatively assess the impact of the old landslide and glacier retreat on the progressive change in slope stability and kinematics would benefit from geomechanical numerical modelling. The complexity of the landslide event, in terms of involved failure mechanisms, structural control, and long-term geomorphic changes (including the older landslide and the glacial retreat) require careful consideration in order to identify the most appropriate numerical method to realistically simulate the event.

The choice between a 2D or a 3D approach is a critical step towards a reliable numerical analysis. In general, a 2D approach may be suited to simulate simple landslides that displace along the line of maximum steepness of the slope, such as roto-translational landslides in soil or, to some extent, planar or wedge landslides in rock with a basal plane or intersection normal to the slope direction, respectively. The structurally-controlled nature of the 2020 Elliot Creek slide calls for a 3D numerical modelling approach in order to account for the varying displacement directions and failure mechanisms of subsequent landslides that affected the slope.

The complexity of the processes that influenced the Elliot Creek slide prior to its failure must also be considered in the choice of numerical method. The selected method should be capable of simulating the effects of the progressive thinning and retreat of the glacier on the slope kinematics, as well as the yielding and rock mass damage accumulation as a result of such changes. Similarly, the effects of the detachment of the older landslide on slope kinematics and progressive damage accumulation should be investigated. The choice of numerical method is also based on the objective of the slope simulation. A landslide investigation that focuses on the pre-failure behavior of the slope, up to the initial detachment of the landslide, may be suited to a continuum approach (e.g., finite element, FEM, or finite difference method, FDM). However, if the numerical modelling is to simulate the landslide behavior from the pre-failure to the deposition stage (i.e., a "total slope failure analysis", Stead et al., 2006), then a method capable of simulating complex block interaction, new contact detection, and, possibly, intact rock fracturing and comminution, should be selected instead. Discontinuum methods (e.g., discrete or distinct element methods, DEM) as well as hybrid, finite-continuum methods (e.g., finite-discrete element method, FDEM) have been successfully employed to simulate structurally controlled landslides involving intra-block fracturing, with the latter specifically developed for such purpose (see Donati et al., 2018, for a review of the methods).

It should be noted that, based on our interpretation, rock mass yielding played an important role in the failure of the Elliot Creek slide, as it is required to allow a rotational displacement to occur. Input data for a numerical modelling analysis would therefore require the collection of additional field data to reliably estimate the strength and deformability of the rock mass involved in the failure.

6 CONCLUSION

On 28 November 2020, an 18 million m^3 rock slide detached from the western slope of the Elliot Creek, entering the Elliot Lake and producing a tsunami wave that propagated at high speed, and built an alluvial fan at the intersection with the Southgate River.

In this research, we used a variety of remote sensing tools, including airborne LiDAR and SfM, to investigate the geomorphic and structural configuration of the landslide rupture surface, and identify the factors that controlled the evolution and kinematics of the landslide.

We performed a multi-scale slope characterization, which included a geomorphic and lineament analysis, as well as rock

mass discontinuity mapping. We noted a strong agreement between the orientation of rock mass discontinuities, slope-scale lineaments, and regional-scale geomorphic features. Our results suggest that the behaviour and evolution of the landslide was controlled by the geological structural configuration of the rock slope.

Our research also showed that the geomorphic evolution of the valley played an important role in the occurrence of the landslide. We suggest that the occurrence of the older landslide was a key event that significantly affected the kinematic configuration of the slope, reducing the support and kinematic constraint, ultimately promoting the mobilization of the 2020 Elliot Creek landslide.

Over the past 60 years, the West Grenville glacier retreated by over 1200 m. In the landslide area, between 1965 and 2019 the elevation of the glacier decreased by about 100 m. Although it is unclear whether such a decrease in ice volume decreased significantly the lateral support provided by the glacier, it is likely that, in the long term, the progressive retreat resulted in an enhanced kinematic freedom for the slope, causing the occurrence of the older landslide, which promoted, in turn, the detachment of the 2020 landslide.

The combined effect of the older landslide, long term slope over steepening due to glacier activity, and, possibly, present-day global warming contributed to the evolution of the rock slope stability, through the long-term change in slope kinematics and the initiation of a progressive failure mechanism which ultimately led to the 2020 event.

DATA AVAILABILITY STATEMENT

The data analyzed in this study is subject to the following licenses/restrictions: LiDAR datasets were collected by Hakai Institute and provided to the authors for the purpose of this research. Requests to access these datasets should be directed to Hakai Institute (https://hakai.org/).

AUTHOR CONTRIBUTIONS

DD, DS, and MG contributed to conception and design of the study. BM provided remote sensing data. DD performed the slope analysis and result interpretation. JB performed the glacier change analysis and compiled the relative paragraph in methodology. DD wrote the first draft of the paper. DS, BM, and LB provided financial support. All authors contributed to manuscript revision, read, and approved the submitted version.

FUNDING

The authors would like to acknowledge financial support provided through a NSERC Discovery Grant (ID: RGPIN 05817) and FRBC Endowment funds provided to DS, Province of BC funding to MG, and funding from NSERC, the Canada Research Chairs Program and the Tula Foundation to BM.

ACKNOWLEDGMENTS

The authors would like to thank the Hakai Institute and the Government of British Columbia for support in the research and provision of LiDAR and aerial photography used in this research. We also acknowledge the Homalco First Nation for granting us permission to complete research on their traditional territory.

REFERENCES

Agisoft LLC (2021). Metashape 1.8. Available at: https://www.agisoft.com/ (Accessed November 20, 2021).

Agliardi, F., Crosta, G., and Zanchi, A. (2001). Structural Constraints on Deep-Seated Slope Deformation Kinematics. *Eng. Geol.* 59, 83–102. doi:10.1016/S0013-7952(00)00066-1

Agliardi, F., Riva, F., Cola, G., Spreafico, M. C., Bourlès, D. L., Braucher, R., et al. (2018). DSGSD to Rockslide Transition at the Saline Ridge (Valfurva, Italy) Constrained by Dating, Remote Sensing and Time-dependent Modelling. *Geophys. Res. Abstr.* 20, 16050. EGU2018-16050.

Badger, T. C. (2002). Fracturing within Anticlines and its Kinematic Control on Slope Stability. *Environ. Eng. Geosci.* 8, 19–33. doi:10.2113/gseegeosci.8.1.19

Böhme, M., Oppikofer, T., Longva, O., Jaboyedoff, M., Hermanns, R. L., and Derron, M.-H. (2015). Analyses of Past and Present Rock Slope Instabilities in a Fjord Valley: Implications for Hazard Estimations. *Geomorphology* 248, 464–474. doi:10.1016/J.GEOMORPH.2015.06.045

Booth, D. B., Troost, K. G., Clague, J. J., and Waitt, R. B. (2003). "The Cordilleran Ice Sheet," in *Developments in Quaternary Science* (Elsevier Science), 17–43. doi:10.1016/S1571-0866(03)01002-9

Brideau, M.-A., and Stead, D. (2012). Evaluating Kinematic Controls on Planar Translational Slope Failure Mechanisms Using Three-Dimensional Distinct Element Modelling. *Geotech. Geol. Eng.* 30, 991–1011. doi:10.1007/s10706-012-9522-5

Clayton, A., Stead, D., Kinakin, D., and Wolter, A. (2017). Engineering Geomorphological Interpretation of the Mitchell Creek Landslide, British Columbia, Canada. *Landslides* 14, 1655–1675. doi:10.1007/s10346-017-0811-1

CloudCompare (2020). CloudCompare 2.11 [GPL Software]. Retrieved from http://www.cloudcompare.org/ (Accessed November 20, 2021).

Colpron, M., Nelson, J. L., and Murphy, D. C. (2007). Northern Cordilleran Terranes and Their Interactions through Time. *GSA Today* 17, 4. doi:10.1130/GSAT01704-5A.1

Cui, Y., Miller, D., Schiarizza, P., and Diakow, L. J. (2017). *British Columbia Ministry of Energy, Mines and Petroleum Resources, British Columbia Geological Survey*. British Columbia Digital Geology, 9. Open File 2017-8. Available at: https://www2.gov.bc.ca/gov/content/industry/mineral-exploration-mining/british-columbia-geological-survey/geology/bcdigitalgeology.

Darvill, C. M., Menounos, B., Goehring, B. M., Lian, O. B., and Caffee, M. W. (2018). Retreat of the Western Cordilleran Ice Sheet Margin during the Last Deglaciation. *Geophys. Res. Lett.* 45 (18), 9710–9720. doi:10.1029/2018GL079419

Denzinger, F., Machguth, H., Barandun, M., Berthier, E., Girod, L., Kronenberg, M., et al. (2021). Geodetic Mass Balance of Abramov Glacier from 1975 to 2015. *J. Glaciol.* 67 (262), 331–342. doi:10.1017/jog.2020.108

Donati, D., Rabus, B., Engelbrecht, J., Stead, D., Clague, J., and Francioni, M. (2021a). A Robust SAR Speckle Tracking Workflow for Measuring and Interpreting the 3D Surface Displacement of Landslides. *Remote Sens.* 13, 3048. doi:10.3390/rs13153048

Donati, D., Stead, D., Brideau, M.-A., and Ghirotti, M. (2021b). Using Pre-failure and Post-failure Remote Sensing Data to Constrain the Three-Dimensional Numerical Model of a Large Rock Slope Failure. *Landslides* 18, 827–847. doi:10.1007/s10346-020-01552-x

Donati, D., Stead, D., Elmo, D., and Borgatti, L. (2019). A Preliminary Investigation on the Role of Brittle Fracture in the Kinematics of the 2014 San Leo Landslide. *Geosciences* 9, 256. doi:10.3390/geosciences9060256

Donati, D., Stead, D., Elmo, D., Sharif, K., Gao, F., Borgatti, L., et al. (2018). "Experience Gained in Modelling Brittle Fracture in Rock," in *2nd US Rock Mechanics/ Geomechanics Symposium* (Seattle, Washington, USA: American Rock Mechanics Association, 13. Paper ARMA 18-821.

Donati, D., Westin, A. M., Stead, D., Clague, J. J., Stewart, T. W., Lawrence, M. S., et al. (2021c). A Reinterpretation of the Downie Slide (British Columbia, Canada) Based on Slope Damage Characterization and Subsurface Data Interpretation. *Landslides* 18, 1561–1583. doi:10.1007/s10346-020-01601-5

Eberhardt, E., Stead, D., and Coggan, J. S. (2004). Numerical Analysis of Initiation and Progressive Failure in Natural Rock Slopes-The 1991 Randa Rockslide. *Int. J. Rock Mech. Min. Sci.* 41, 69–87. doi:10.1016/S1365-1609(03)00076-5

Fullin, N., Ghirotti, M., Donati, D., and Stead, D. (2021). *Characterising the Kinematics of the Joffre Peak Landslides Using a Combined Numerical Modeling-Remote Sensing Approach*. (EGU General Assembly 2021), EGU21-154. doi:10.5194/egusphere-egu21-154

Geertsema, M., Menounos, B., Bullard, G., Carrivick, J. L., Clague, J. J., Dai, C., et al. (2022). The 28 November 2020 Landslide, Tsunami, and Outburst Flood - A Hazard Cascade Associated with Rapid Deglaciation at Elliot Creek, British Columbia, Canada. *Geophys. Res. Lett.* 49, 6. doi:10.1029/2021GL096716

Gehrels, G., Rusmore, M., Woodsworth, G., Crawford, M., Andronicos, C., Hollister, L., et al. (2009). U-Th-Pb Geochronology of the Coast Mountains Batholith in North-Coastal British Columbia: Constraints on Age and Tectonic Evolution Coast Mountains Batholith. *Geol. Soc. Am. Bull.* 121, 1341–1361. doi:10.1130/B26404.1

Goodman, R. E. (1995). Block Theory and its Application. *Géotechnique* 45, 383–423. doi:10.1680/geot.1995.45.3.383

Goodman, R. E., and Shi, G. (1985). *Block Theory and its Application to Rock Engineering*. Englewood Cliff, New Jersey: Prentice-Hall.

Grämiger, L. M., Moore, J. R., Gischig, V. S., Ivy-Ochs, S., and Loew, S. (2017). Beyond Debuttressing: Mechanics of Paraglacial Rock Slope Damage during Repeat Glacial Cycles. *J. Geophys. Res. Earth Surf.* 122, 1004–1036. doi:10.1002/2016JF003967

Griffiths, J. S., Stokes, M., Stead, D., and Giles, D. (2012). Landscape Evolution and Engineering Geology: Results from IAEG Commission 22. *Bull. Eng. Geol. Environ.* 71, 605–636. doi:10.1007/s10064-012-0434-7

Havaej, M., Stead, D., Eberhardt, E., and Fisher, B. R. (2014). Characterization of Bi-planar and Ploughing Failure Mechanisms in Footwall Slopes Using Numerical Modelling. *Eng. Geol.* 178, 109–120. doi:10.1016/j.enggeo.2014.06.003

Holland, S. S. (1976). *Landforms of British Columbia, A Physiographic Outline*. Canada: Government of the Province of British Columbia, 136. Bulletin 48.

Holm, K., Bovis, M., and Jakob, M. (2004). The Landslide Response of Alpine Basins to Post-little Ice Age Glacial Thinning and Retreat in Southwestern British Columbia. *Geomorphology* 57, 201–216. doi:10.1016/S0169-555X(03)00103-X

Hugonnet, R., McNabb, R., Berthier, E., Menounos, B., Nuth, C., Girod, L., et al. (2021). Accelerated Global Glacier Mass Loss in the Early Twenty-First Century. *Nature* 592, 726–731. doi:10.1038/s41586-021-03436-z

Hungr, O., and Amann, F. (2011). Limit Equilibrium of Asymmetric Laterally Constrained Rockslides. *Int. J. Rock Mech. Min. Sci.* 48, 748–758. doi:10.1016/j.ijrmms.2011.04.008

Hungr, O., Leroueil, S., and Picarelli, L. (2014). The Varnes Classification of Landslide Types, an Update. *Landslides* 11, 167–194. doi:10.1007/s10346-013-0436-y

Kemeny, J. (2005). Time-dependent Drift Degradation Due to the Progressive Failure of Rock Bridges along Discontinuities. *Int. J. Rock Mech. Min. Sci.* 42, 35–46. doi:10.1016/j.ijrmms.2004.07.001

Kos, A., Amann, F., Strozzi, T., Delaloye, R., Ruette, J., and Springman, S. (2016). Contemporary Glacier Retreat Triggers a Rapid Landslide Response, Great Aletsch Glacier, Switzerland. *Geophys. Res. Lett.* 43 (12), 466474. doi:10.1002/2016GL071708

Larsen, I. J., and Montgomery, D. R. (2012). Landslide Erosion Coupled to Tectonics and River Incision. *Nat. Geosci.* 5 (5), 468–473. doi:10.1038/ngeo1479

Leith, K., Moore, J. R., Amann, F., and Loew, S. (2014). Subglacial Extensional Fracture Development and Implications for Alpine Valley Evolution. *J. Geophys. Res. Earth Surf.* 119, 62–81. doi:10.1002/2012JF002691

McColl, S. T., Davies, T. R. H., and McSaveney, M. J. (2010). "Glacier Retreat and Rock-Slope Stability: De-bunking Debuttressing," in *Geologically Active: 11th Congress of the International Association for Engineering Geology and the Environment* (Auckland, New Zealand: CRC Press, 467–474. Available at: https://www.routledge.com/Geologically-Active-Proceedings-of-the-11th-IAEG-Congress-Auckland-New/Williams-Pinches-Chin-McMorran-Massey/p/book/9780415600347.

McNabb, R., Nuth, C., Kääb, A., and Girod, L. (2019). Sensitivity of Glacier Volume Change Estimation to DEM Void Interpolation. *Cryosphere* 13, 895–910. doi:10.5194/TC-13-895-2019

Menounos, B., Goehring, B. M., Osborn, G., Margold, M., Ward, B., Bond, J., et al. (2017). Cordilleran Ice Sheet Mass Loss Preceded Climate Reversals Near the Pleistocene Termination. *Science* 358, 781–784. doi:10.1126/SCIENCE.AAN3001

Menounos, B., Hugonnet, R., Shean, D., Gardner, A., Howat, I., Berthier, E., et al. (2019). Heterogeneous Changes in Western North American Glaciers Linked to Decadal Variability in Zonal Wind Strength. *Geophys. Res. Lett.* 46, 200–209. doi:10.1029/2018GL080942

Monger, J. W. H., Price, R. A., and Tempelman-Kluit, D. J. (1982). Tectonic Accretion and the Origin of the Two Major Metamorphic and Plutonic Welts in the Canadian Cordillera. *Geol* 10, 70. doi:10.1130/0091-7613(1982)10<70:taatoo>2.0.co;2

Nuth, C., and Kääb, A. (2011). Co-registration and Bias Corrections of Satellite Elevation Data Sets for Quantifying Glacier Thickness Change. *Cryosphere* 5, 271–290. doi:10.5194/TC-5-271-2011

Pelto, B. M., Menounos, B., and Marshall, S. J. (2019). Multi-year Evaluation of Airborne Geodetic Surveys to Estimate Seasonal Mass Balance, Columbia and Rocky Mountains, Canada. *Cryosphere* 13 (6), 1709–1727. doi:10.5194/TC-13-1709-2019

Riva, F., Agliardi, F., Amitrano, D., and Crosta, G. B. (2018). Damage-based Time-dependent Modeling of Paraglacial to Postglacial Progressive Failure of Large Rock Slopes. *J. Geophys. Res. Earth Surf.* 123, 124–141. doi:10.1002/2017JF004423

Rocscience (2016). SWEDGE, Version 6. Available at: www.rocscience.com (Accessed November 20, 2021).

Roddick, J. A., and Woodsworth, G. J. (2006). *Bute Inlet, British Columbia/Geology by J.A. Roddick [and Others] ; Compiled by J.A. Roddick and G.J. Woodsworth*. Canada: Geological Survey. doi:10.4095/221570

Rupnik, E., Daakir, M., and Pierrot Deseilligny, M. (2017). MicMac - a Free, Open-Source Solution for Photogrammetry. *Open Geospatial Data, Softw. Stand.* 2, 1–9. doi:10.1186/S40965-017-0027-2

Stead, D., Donati, D., and Brideau, M.-A. (2022). "Rock Slides and Topples," in *Treatise on Geomorphology*. Editor J. F. Shroder (Academic Press). Second Edition, 114–136. doi:10.1016/B978-0-12-818234-5.00060-2

Stead, D., Eberhardt, E., and Coggan, J. S. (2006). Developments in the Characterization of Complex Rock Slope Deformation and Failure Using Numerical Modelling Techniques. *Eng. Geol.* 83 (1-3), 217–235. doi:10.1016/j.enggeo.2005.06.033

Stead, D., and Wolter, A. (2015). A Critical Review of Rock Slope Failure Mechanisms: the Importance of Structural Geology. *J. Struct. Geol.* 74, 1–23. doi:10.1016/j.jsg.2015.02.002

Umhoefer, P. J., and Miller, R. B. (1996). Mid-Cretaceous Thrusting in the Southern Coast Belt, British Columbia and Washington, after Strike-Slip Fault Reconstruction. *Tectonics* 15, 545–565. doi:10.1029/95TC03498

Whalley, W. B. (1974). *The Mechanics of High-Magnitude, Low-Frequency Rock Failure and its Importance in a Mountainous Area*. Reading, UK: University of Reading, Department of Geography. Paper 27.

Wolter, A., Gischig, V., Stead, D., and Clague, J. J. (2016). Investigation of Geomorphic and Seismic Effects on the 1959 Madison Canyon, Montana, Landslide Using an Integrated Field, Engineering Geomorphology Mapping, and Numerical Modelling Approach. *Rock Mech. Rock Eng.* 49, 2479–2501. doi:10.1007/s00603-015-0889-5

Conflict of Interest: The authors declare that the research was conducted in the absence of any commercial or financial relationships that could be construed as a potential conflict of interest.